Semicond. Sci. Technol. **23** (2008) 035023 (10pp) doi:10.1088/0268-1242/23/3/035023

# Effects of defects in semiconductors on reproducibility and performance of thin-film photovoltaic solar cells

**I M Dharmadasa, G J Tolan and M Cazaux**

Materials & Engineering Research Institute, Faculty of Arts, Computing, Engineering and Sciences, Sheffield Hallam University, Sheffield S1 1WB, UK

E-mail: Dharme@shu.ac.uk

Received 25 September 2007, in final form 11 December 2007
Published 18 February 2008
Online at stacks.iop.org/SST/23/035023

**Abstract**

Thin-film solar cells based on GaAs/$Al_xGa_{(1-x)}As$ showing open circuit voltages of (1100–1170) mV and fill factors of (0.80–0.87) have been exposed to external electrical stresses, and current–voltage characteristics were monitored in order to study the effects of defects present in the device structure. It has been found that peculiar kinks, sudden jumps and various deformations occur in current–voltage curves which could be caused when the Fermi level moves position at the device interface. These changes occur when there is a group of defect levels and the Fermi level is forced to move across these levels. The reproducibility and performance of solar cells heavily depend on the properties of these defect structures, and external forces such as electrical stresses, illumination and temperature variations cause changes in the measured current–voltage characteristics. The observed variations during this work together with examples from the literature are presented and discussed in this paper. It is concluded that the control of these defects present in device structures is crucial in developing stable, durable and high-efficiency thin-film solar cells.

(Some figures in this article are in colour only in the electronic version)

## Introduction

The worldwide photovoltaic (PV) research efforts are currently devoted to the production of low-cost and high-efficiency solar cells for conversion of sunlight directly into electricity. Several different systems are under research and some development stages have been successfully commercialised already. All-solid and inorganic PV solar cells are based on crystalline, polycrystalline and amorphous silicon, III–V compounds and polycrystalline CdTe and $CuInGaSe_2$ (CIGS) thin films.

Further progress in this field is required in order to cut the PV cost and increase the conversion efficiencies. The PV market is currently filled with silicon, CdTe and CIGS solar panels. However, there are some issues with thin-film solar cells, especially on reproducibility, variations in performance, stability and lifetime. In the assessment of solar panels and monitoring of the performance, strange behaviour of *I–V* characteristics has been observed. The light soaking effects, change of *I–V* characteristics when measurements are repeated and other unusual behaviours during temperature changes have been experimentally observed. Some of these variations and behaviours are not understood at present, and this experimental work was launched to explore these unusual behaviours. Possible explanations to these changes and some solutions to reduce these undesirable behaviours have been presented in this paper.

The experimental work and discussions presented here are based on the observation of defect structures present in thin-film solar cells. The recently proposed new scientific model (Dharmadasa *et al* 2002) has shown the effect of several defect levels on CdTe solar cells, and these ideas have also been extended to CIGS-based solar cells (Dharmadasa *et al* 2005a). Developing the new ideas further, multi-layer graded bandgap solar cell structures have been proposed (Dharmadasa *et al* 2004, 2005b), and these concepts have been experimentally tested and proven using a well-researched GaAs/$Al_xGa_{(1-x)}As$ alloy system (Dharmadasa *et al* 2005a, 2006). This work has produced solar cells with open circuit voltages of

 

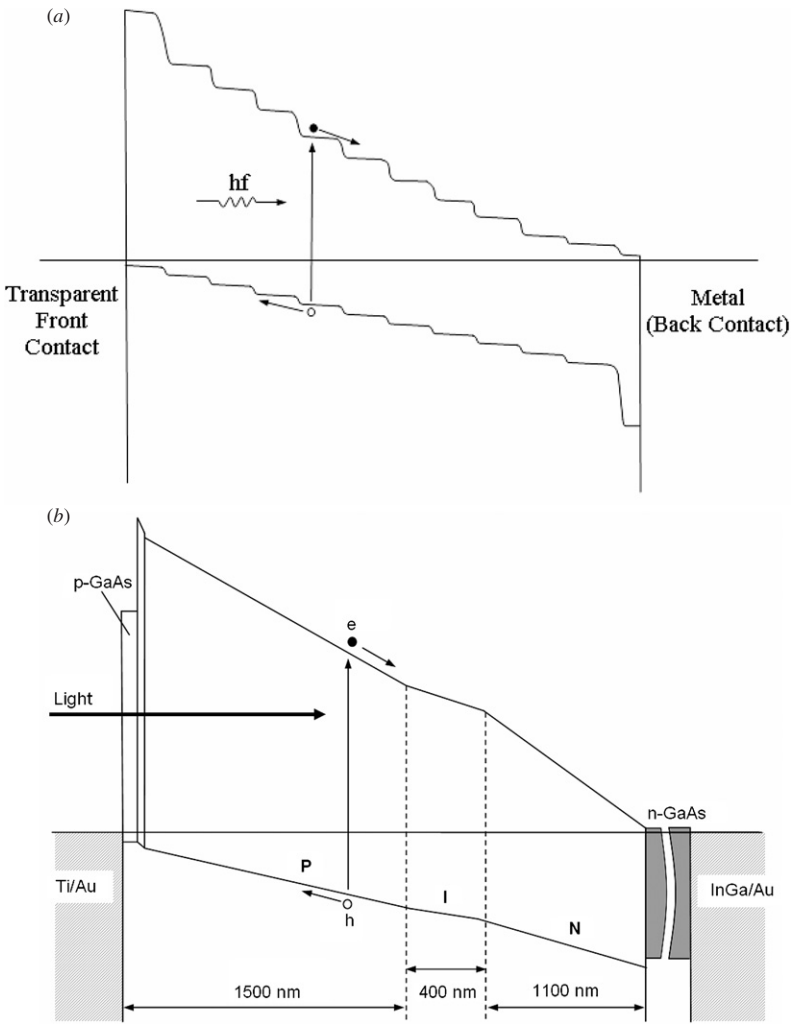


**Figure 1.** Idealized design for multi-layer graded bandgap solar cells (*a*), and the closest sketch of the energy band diagram for $Al_xGa_{(1-x)}As/GaAs$ solar cells (b) studied in this work.

(1100–1170) mV and fill factors of (0.80–0.87), exceeding highest reported values of 1022 mV (Green *et al* 2005) and 1047 mV (Takahashi *et al*) for the $Al_xGa_{(1-x)}As/GaAs$ system. The above solar cell parameters have been independently measured in five different laboratories for comparison and confirmation (Dharmadasa *et al* 2006). These solar cells with high performance parameters have been used in this work to explore the measurement variations and stability issues commonly observed for thin-film solar cells.

## Experimental procedure and results

The energy band diagram shown by figure 1(*a*) has been selected for the production of multi-layer graded bandgap solar cell structures (Dharmadasa 2005). Well-researched GaAs and $Al_xGa_{(1-x)}As$ materials grown by MOCVD technique were used to produce the main features shown by this energy band diagram, starting from the n-type GaAs substrate. The bandgap was increased gradually by adding more aluminium into the alloy system, and the electrical conductivity type was changed from n-type to p-type by varying the concentration of Si and C dopants, respectively. A thin layer of p-type GaAs was used as a capping layer to avoid oxidation of aluminium and this layer was removed during the processing of these initial devices. The closest sketch of the energy band diagram of this device structure is given in figure 1(*b*) and the total thickness of the solar cell structure was made to be about 3 $\mu$m. The MOCVD growth was only possible with gradual increase of Al contact in the material. Although the exact shapes of the two band diagrams shown in figure 1(*a*) and (*b*) are slightly different, the main features remain the same. In particular the variation of the electrical conduction type from p- to n- and the gradual reduction of the bandgap from the front to the back of the solar cell have been kept in a similar way. The lab scale devices were processed as described in a previous publication (Dharmadasa *et al* 2005a). Devices with a 0.5 mm diameter and 3 × 3 $mm^2$, 5 × 5 $mm^2$ and 10 × 10 $mm^2$ contacts were fabricated for the assessment of these solar cells. The areas of the two types of devices used in this work were 0.002 $cm^2$ (0.5 mm diameter dots) and 0.090 $cm^2$

**Table 1.** Typical solar cell parameters measured under AM1.5 conditions for 0.002 $cm^2$ and 0.090 $cm^2$ solar cells.

| Device | | $V_{oc}$ (mV) | $J_{sc}$ (mA $cm^{-2}$) | FF (%) | $\eta$ (%) | $R_s$ ($\Omega$ $cm^2$) | $R_p$ ($\Omega$ $cm^2$) |
|---|---|---|---|---|---|---|---|
| 0.002 $cm^2$ solar cells | 1 | 1110 | 12.1 | 83 | 11.2 | – | – |
| | 2 | 1081 | 12.3 | 82 | 11.0 | 2.3 | 4200 |
| | 3 | 1077 | 12.3 | 82 | 10.8 | 2.9 | 3000 |
| 0.090 $cm^2$ solar cells | 1 | 1148 | 11.9 | 86 | 11.7 | 2.5 | 10 400 |
| | 2 | 1141 | 11.4 | 86 | 11.2 | 4.0 | 5100 |
| | 3 | 1150 | 13.1 | 85 | 12.7 | 3.8 | – |

**Table 2.** Summary of solar cell parameters observed as a function of application of external electrical stress, for a 0.5 mm diameter cell (see figure 5(*b*)).

| Test no. | Action | $V_{oc}$ (mV) | FF (%) | $I_{sc}$ (mA) | $J_{sc}$ (mA $cm^{-2}$) |
|---|---|---|---|---|---|
| 0 | First measurement | 1093 | 84 | 0.036 | 18.0 |
| 1 | Forward bias 2 h with 1 V | 930 | 73 | 0.037 | 18.3 |
| 2 | Forward bias 3 h with 1 V | 855 | 77 | 0.023 | 11.4 |
| 3 | Reverse bias 17 h with 0.7 V | 855 | 74 | 0.032 | 16.1 |
| 4 | Reverse bias 3 h with 0.8 V | 888 | 77 | 0.021 | 10.7 |
| 5 | Reverse bias 19 h with 0.8 V | 1038 | 83 | 0.012 | 6.0 |
| 6 | Reverse bias 3 h with 0.8 V | 963 | 54 | 0.045 | 2.2 |
| 7 | Reverse bias 19 h with 0.8 V | 1081 | 81 | 0.028 | 14.1 |
| 8 | Forward bias 66 h with 0.9 V | 1050 | 82 | 0.016 | 7.8 |
| 9 | Forward bias 28 h with 0.9 V | 625 | 62 | 0.024 | 12.0 |
| 10 | Forward bias 25 h with 0.9 V | 1025 | 80 | 0.009 | 4.6 |

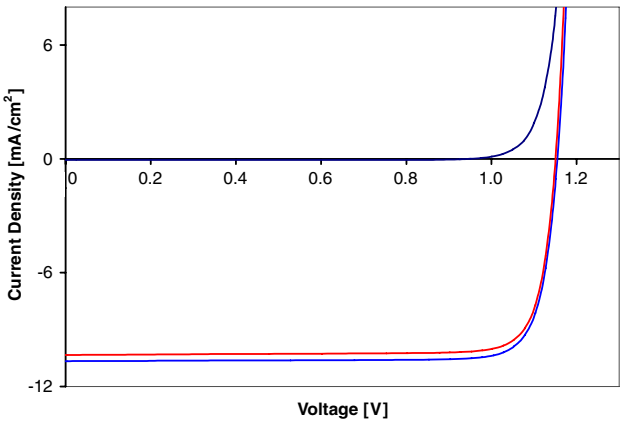


**Figure 2.** Current–voltage characteristics measured for two 3 × 3 $mm^2$ solar cells, under AM1.5 conditions. Only one dark *I–V* curve is shown for clarity and the other curve is very similar.

(3 × 3 $mm^2$). The 3 × 3 $mm^2$ devices also had 120 nm thick $MgF_2$ anti-reflection coating.

The performance of these solar cells was tested under AM1.5 illumination, and the results were compared and confirmed by measuring in five different laboratories (Dharmadasa *et al* 2006) (Sheffield Hallam University and South Bank University in the UK, Zürich and Lausanne groups in Switzerland and NREL in USA). A typical set of *I–V* characteristics for 3 × 3 $mm^2$ solar cells are shown in figure 2 and some measured parameters are summarized in table 1. It has been observed that the fill factors of these devices are above 0.80, and the highest measured $V_{oc}$ value is 1170 mV. The performance of 3 × 3 $mm^2$ solar cells is better than that of the first set of 0.5 mm diameter devices due to removal of the more GaAs capping layer and the addition of an anti-reflection coating. As shown in figure 2, the *I–V* characteristics shows excellent properties, and these diodes were selected for studying the effects of defects in solar cells.

The devices selected were first measured for their solar cell parameters ($V_{oc}$, $J_{sc}$ and FF), and then electrical stresses were applied while the devices were kept at room temperature and in dark conditions. For example, the diodes were forward biased (FB) with voltages up to ∼1.0 V, for several hours, and *I–V* curves were measured immediately after removal of the bias voltage. The same diodes were then exposed to reverse bias (RB) conditions with voltage of ∼0.8 V, for several hours, and *I–V* curves were recorded immediately. Both the forward and reverse bias voltages were chosen in order to sweep the full band gap, but not to cause any electrical or thermal breakdown of the diode during applied bias over a long period. Drastic changes in *I–V* characteristics have been observed even in these high quality solar cells, very similar to the reported work on metal/n-CdTe interfaces (Dharmadasa *et al* 2005a). Typical results are summarized in table 2 and shown in figures 3–6.

During subsequent *I–V* measurements after applying electrical stresses to device structures, *I–V* curves showed peculiar kinks as shown in figure 3, sudden discontinuities as shown in figure 4(*a*) and unusual characteristics as shown in figure 4(*b*). Figure 5 graphically summarizes the variation of $V_{oc}$ and FF values observed after various conditions applied to two 0.5 mm diameter solar cells. Detailed parameters observed for one diode are presented in table 2. Figure 6 summarizes similar results obtained for two 3 × 3 $mm^2$ solar cells.

## Discussion of results

Before discussing these observed results for metal/$Al_xGa_{(1-x)}As$/GaAs/metal diodes, it is worth summarizing

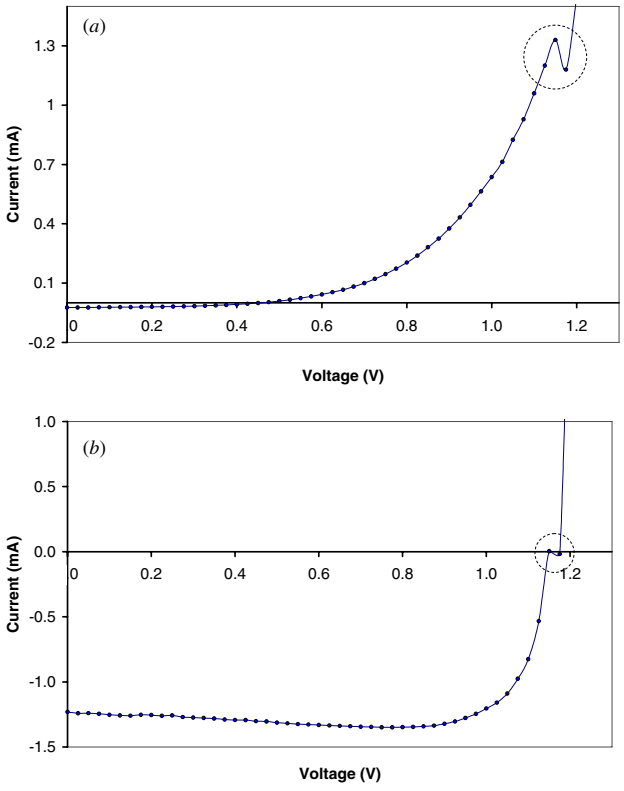


**Figure 3.** Kinks observed during *I–V* measurements of 0.5 mm diameter solar cells after applying various electrical stresses to the diode. These kinks appear randomly at different places of the *I–V* curve.

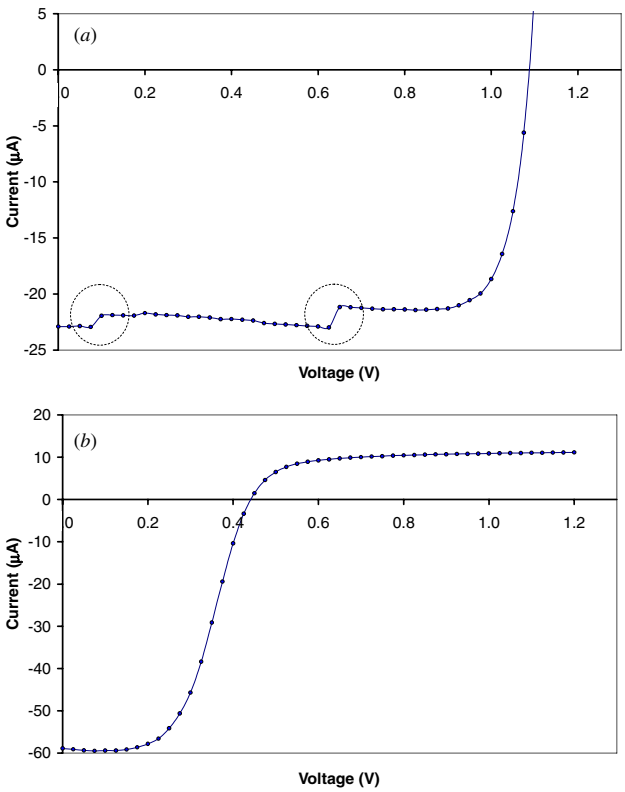


**Figure 4.** Sudden discontinuities (*a*), and completely distorted *I–V* curves (*b*), observed during measurements after applying external electrical stresses to diodes and then removed.

the recently reported work on metal/n-CdTe single interfaces in the presence of a set of defects labelled from $E_1$ to $E_5$ (Dharmadasa *et al* 2005a). The different situations for metal/n-CdTe interfaces are shown in figure 7, and the three diagrams represent zero bias, forward bias and the reverse bias conditions, respectively. Forward bias conditions allow trap levels to fill and reverse bias allows these levels to empty due to their relative positions with respect to the Fermi level. Also, the forward bias condition is equivalent to the open circuit situation of a solar cell under illumination or the solar panel used during the day time. During night time, a solar cell has the zero bias condition and hence the defects situated above the Fermi level will de-trap during dark conditions. This work has demonstrated that the forward bias or illumination of active junctions with existing defect structures could produce lower potential barriers or lower $V_{oc}$ values and hence low conversion efficiencies (results are shown in table 2 and figures 5 and 6). These conditions can be reversed for some devices by applying reverse bias voltages leaving the devices under dark conditions for several hours.

Similar situations may arise when *I–V* measurements are repeated within a period of a few minutes. For example, during an *I–V* curve measurement cycle, say between –1 and +1 V, the Fermi level moves at the interface from forward bias to reverse bias or vice versa. In the presence of a set of deep traps at the interface, the Fermi level crosses these levels and allow them to trap or de-trap electrons according to the situation. This will in turn allow the Fermi level to switch between defect levels and hence affect the potential barrier height and the properties of *I–V* characteristics measured. It should be noted that these changes are affected by the immediate history of the device such as ambient temperature, illumination conditions, etc.

It is now appropriate to discuss the defect levels present at the two interfaces of the device under investigation. Defects on both GaAs (EMIS Data Review 1990, Hashizume and Nagabuchi 1989) and $Al_xGa_{(1-x)}As$ (Adachi 1993, Darmo *et al* 1998) layers have been thoroughly studied in the past, and the main electron traps are shown in figure 8. As described before, these defect structures can drastically affect the *I–V* characteristics of the device. For example, when the Fermi level sweeps along the metal/$Al_xGa_{(1-x)}As$ interface during the *I–V* measurement cycle, or during application of electrical stresses, the Fermi level could move onto different positions, producing diodes of different barrier heights. These device structures with numerous defect levels at their interfaces, therefore, could produce different *I–V* characteristics depending on the immediate history of the device. Some of the possible different *I–V* curves are shown with dotted lines in figure 9 with different potential barriers, and during the switch over from one *I–V* curve to another; peculiar kinks and sudden discontinuities could occur as shown in the diagram. These kinks and discontinuities could appear at different positions depending on the defect structures, defect densities and their electron occupation.

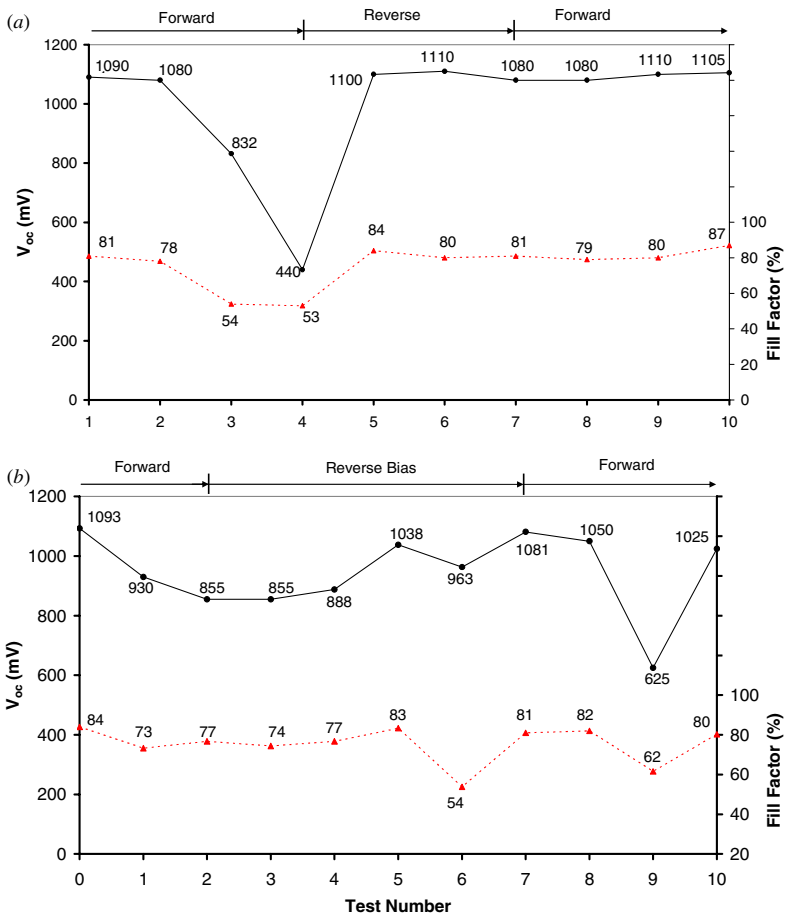


**Figure 5.** The variation of $V_{oc}$ and FF as a function of application of forward and reverse-biased electrical stresses on two 0.5 mm diameter solar cells.

Since this diode has two interfaces with complex defect structures, the Fermi level crosses defect levels on both the interfaces. When the right conditions have been established, it is possible to shift the Fermi level position to form a distorted energy band diagram as shown in figure 10. For example, the application of reverse bias stress to this device structure and removal could easily trigger the Fermi level shift to a lower position at the $Al_xGa_{(1-x)}As/GaAs$ interface. When this happens, there are two diodes in the device structure connected opposite to each other, and a typical *I–V* curve represented by figure 4(*b*) will be the final result. This situation corresponds to the test number 4 of figure 5(*a*), and note the drastic reduction of solar cell parameters ($V_{oc} \sim 440$ mV and FF $\sim 0.53$) due to the weakened main diode. At large forward bias voltages, the main diode reaches flat-band conditions, and the reverse bias properties of smaller diode at $Al_xGa_{(1-x)}As/GaAs$ interface dominates *I–V* characteristics showing its saturation current in the first quadrant.

Figure 5(*a*) represents a clear example of reduction of $V_{oc}$ as a result of forward biasing, and reversal to the original value after reverse biasing. With further forward biasing, this particular diode (0.5 mm diameter dot) shows stable behaviour after this first variation indicating a permanent change such as a removal or passivation of temporary defects existing at the interface. This type of temporary defects may arise due to trapped charges at the interface. On the other hand, the diode shown by figure 5(*b*) shows a reversible behaviour. Forward bias reduces $V_{oc}$ and reverse bias recovers the value to original figures with $V_{oc}$ again reducing after further forward biasing. This behaviour seems reversible for this diode indicating the presence of a set of permanent defect structures at the interface.

The results shown by figure 6 for $3 \times 3$ mm$^2$ solar cells seem to be very stable showing the most desirable qualities needed for a practical solar cell. These $3 \times 3$ mm$^2$ solar cells have a thinner p-GaAs capping layer when compared to 0.5 mm diameter cells and a 120 nm thick $MgF_2$ anti-reflection coating. Less amount of unwanted p-GaAs layers and the anti-reflection coating may have improved the device parameters. Also the sealing effect by $MgF_2$ may also have reduced the amounts of detrimental defects at this interface to reduce these undesirable fluctuations.

It should be noted that filling and emptying of defect levels are also influenced by changes in temperature and light intensity in addition to the electrical stresses externally applied to the device. Therefore, the results may vary according to the dominant effect in a particular situation. The deterioration of $V_{oc}$ during day time, or the light soaking (equivalent to forward biasing effect) and recovery effect during night time

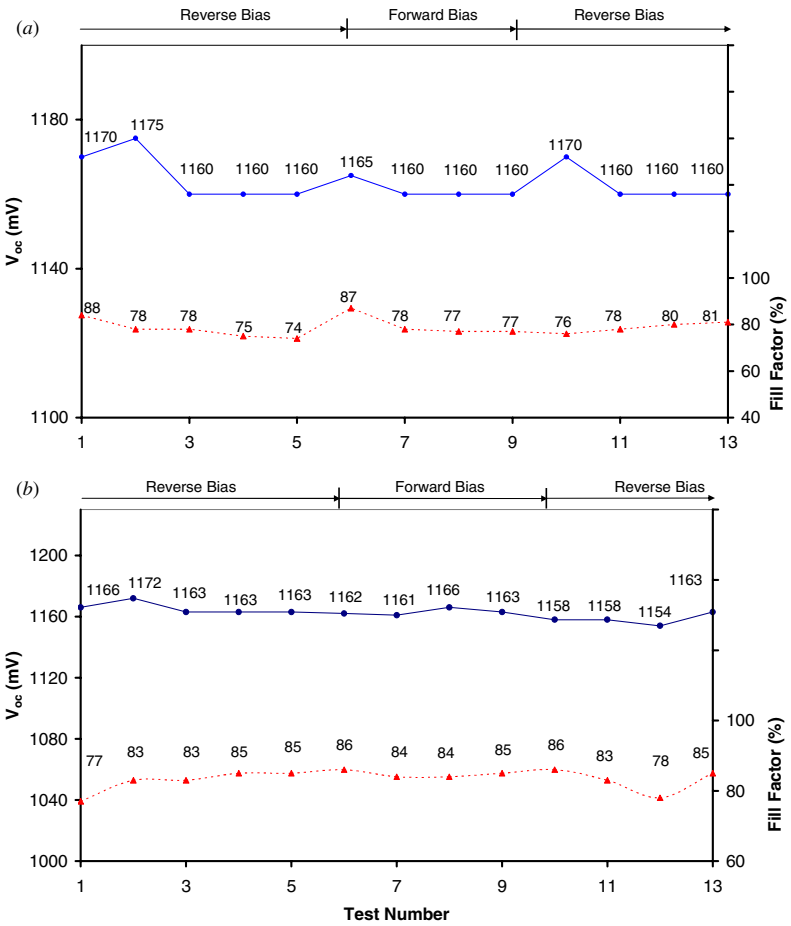


**Figure 6.** The variation of $V_{oc}$ and FF as a function of application of forward- and reverse-biased electrical stresses on two 3 × 3 mm$^2$ solar cells.

(equivalent to zero bias situation) observed for all kinds of thin-film solar cells can be explained in terms of defects in the semiconductors or at the interfaces. The removal or passivation of unwanted defects in solar cells will allow production of high-efficiency solar cells and reduce these undesirable instability effects.

During these experiments, the magnitude of both forward and reverse voltages was carefully selected in order to keep the Joule heating and possible electric breakdown to a minimum. The bias voltages are selected simply to shift the Fermi level so that defect levels can be filled (forward bias) or emptied (zero or reverse bias) during a bias period. We have also changed the duration of the bias gradually until noticeable changes have taken place. The correlation between bias voltage and duration of bias is a difficult task, since thermal effects, exposure to light before measurements and the nature of defects (slow or fast) are all unknown factors. These experiments were mainly aimed to explore the trends, and find out why solar cell measurements are variable and sometimes not reliable in normal laboratory measurement conditions.

Comprehensive work on electrodeposited CdTe- and CIGS-based solar cells in the authors' group also showed *I–V* curves of different shapes for different batches of devices. These different types of *I–V* curves are sketched in figure 11 to help the discussion, and three major groups are labelled as curves A, B and C. Curve A represents the desired solar cell characteristics, observed when the defect concentrations are low or non-existent in the device structure. The other extreme is shown by curve C where the photo-generated charge carriers are removed drastically by defects through recombination and generation (R&G) process and hence the current in the external circuit is low and the fill factor reduces drastically. The amount of R&G varies according to the defect structure present, defect's location and concentrations and the Fermi level position at the interface. Depending on the circumstances, any shape between A and C could be measured. A special situation shown by curve B is also observed but this linear behaviour is only one of the possibilities and not due to higher series resistance of the device structure. Similar results have been reported by Platzer-Björkman *et al* (2003) for solar cells based on CIGS grown by the vacuum-evaporated method.

The unstable behaviour of Showa-Shell CIGS solar panels, as reported by Kushiya (2004) is another good example. Although these Showa-Shell CIGS panels produced world highest large area module efficiencies in 2003 (Kushiya 2003), major features of instability are shown in figure 12. It is clear that the light soaking of solar panels reduces the efficiency from ∼13% to ∼8.5%. However, cooling during an

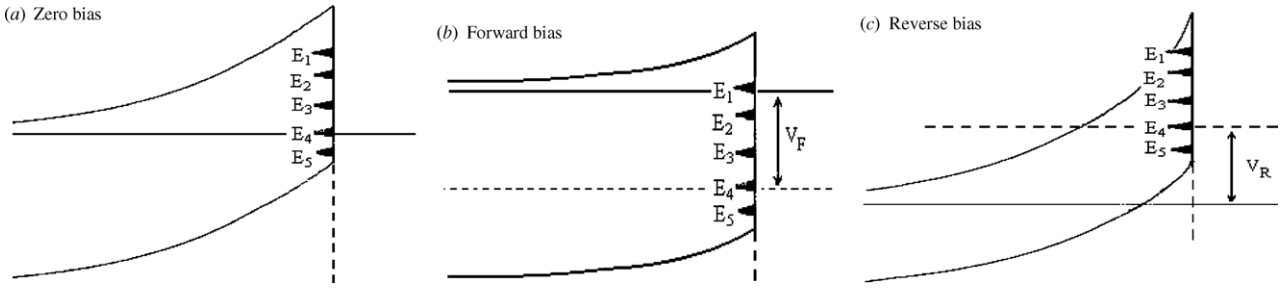


**Figure 7.** The experimentally observed five Fermi level pinning positions at a metal/n-CdTe interface. (a) At zero bias, the Fermi level is pinned at level $E_4$, (b) application of forward bias, $V_F$, across the diode starts to fill $E_1 \rightarrow E_4$ levels with electrons, (c) application of reverse bias starts to empty electrons from $E_1 \rightarrow E_5$ and when released the Fermi level pinning may return to the most probable $E_5$ or $E_4$ levels, depending on the amount of de-trapping taken place.

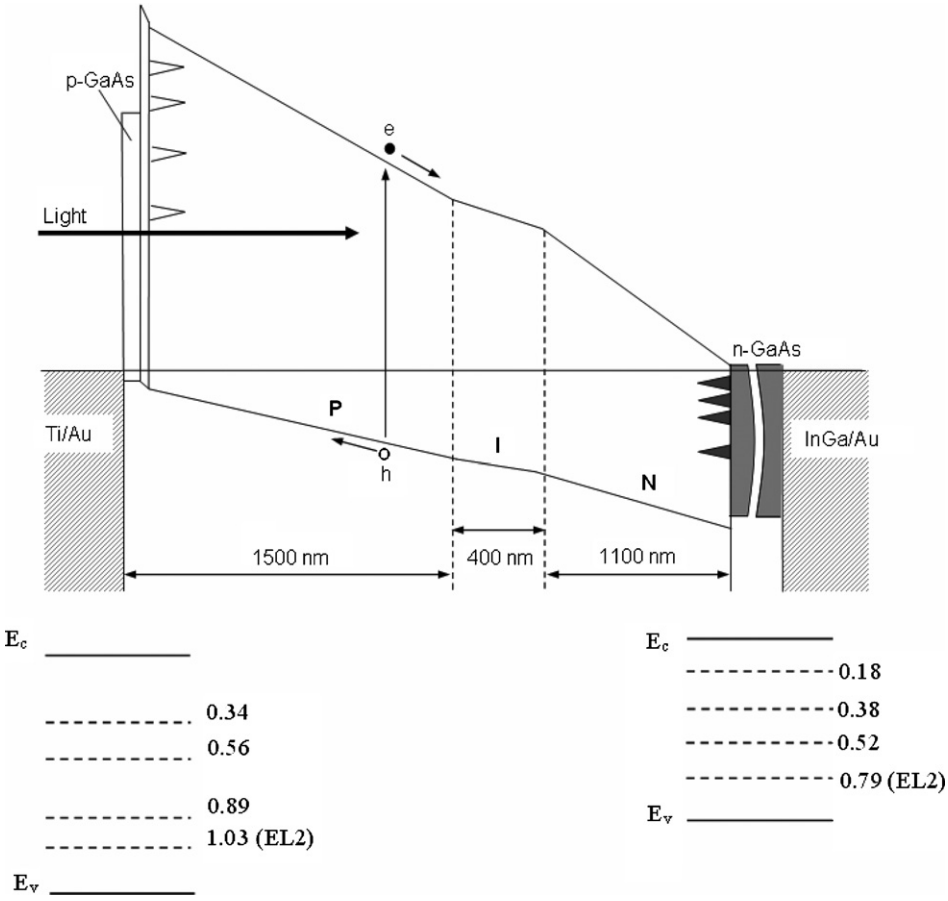


**Figure 8.** Sketch of the energy band diagram of $Al_xGa_{(1-x)}As/GaAs$ solar cell together with well-established defect levels present at metal/$Al_xGa_{(1-x)}As$ and $Al_xGa_{(1-x)}As/GaAs$ interfaces.

*I–V* test increases the efficiency back to its maximum values of ∼13%. This is mainly due to the quenching of R&G activities by freezing defect activities at lower temperatures. The presence of a set of defect levels in the Showa-Shell CIGS material has been experimentally observed and recently reported by the authors' group (Dharmadasa *et al* 2005a). The identification of the origin of these defect levels and their removal or passivation will eliminate these undesirable instability issues and produce stable and high efficiency thin-film solar panels.

The usually observed trade-off between the two parameters $V_{oc}$ and $J_{sc}$ can also be understood in terms of defect structures present in solar cells. The most recent report by Contreras *et al* (2005) together with the general observation of improved $V_{oc}$ values with corresponding reduced $J_{sc}$ could be explained as follows. Whatever the device structure used, there exists an active photo-voltaic junction, with a set of defect levels. As an example, consider the simplest situation shown by figure 7. The following explanations are equally applicable for any other junctions based on p-type or n-type

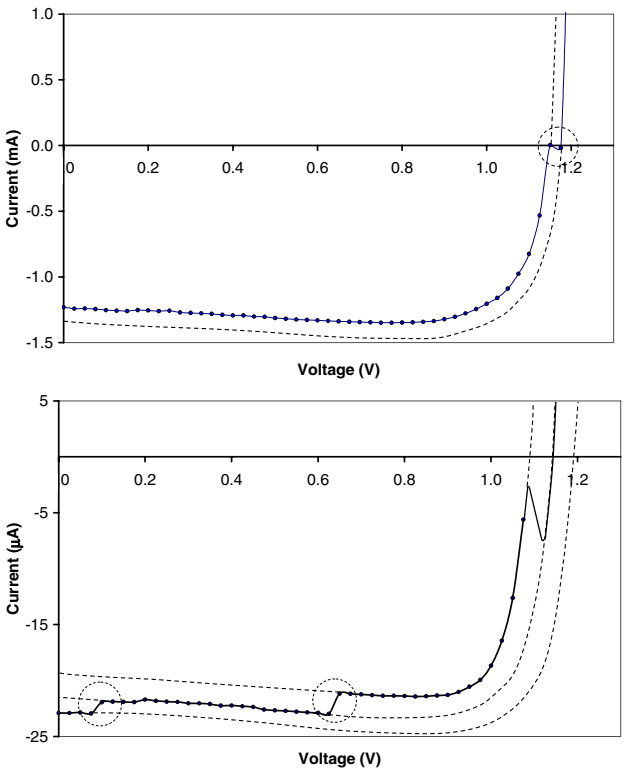


**Figure 9.** Kinks and sudden discontinuities observed in *I–V* curves show the Fermi level changes from one position to another producing different *I–V* characteristics corresponding to different potential barrier heights.

semiconductors. Let us consider a solar cell based on a metal/semiconductor interface with five defect levels present, as shown in figure 7. The R&G is highest due to $E_3$ level situated in the middle of the bandgap. In the case of Fermi level pinning at $E_4$ or $E_5$ levels, high $V_{oc}$ values are obtained, but the R&G is extremely high due to actions of empty $E_3$ level. The ultimate result is the observation of a high $V_{oc}$ with a low $J_{sc}$ value. On the other hand, if the Fermi level is located just above $E_3$ (say pinned at $E_2$), the results will be a low $V_{oc}$ value but a drastic reduction of R&G activities occur due to the filled or saturated $E_3$ level. When there is sufficient band bending to collect photo-generated charge carriers due to Fermi level pinning above $E_3$ level, a low $V_{oc}$ and a high $J_{sc}$ will be the final result. However, depending on the situation, due to drastic reduction of band bending low $J_{sc}$ could also be observed with low $V_{oc}$ values.

A large body of experimental evidence published on amorphous and polycrystalline silicon solar cells also show degradation due to light soaking (Smirnov *et al* 2004, Nobile and Morana 2003). There are also numerous reports in the literature on solar panel degradation during the day time and recovery during the night time. These behaviours are identical to properties explained in this paper on solar cells based on CdTe, CIGS and $Al_xGa_{(1-x)}As$. This commonality in all thin-film solar cells highlights the importance of the effects of defects in semiconductors on the performance and reliability of solar panels. As the absorber layer of the thin-film solar panels gets thinner, the effects of defects at the two surfaces are going to be drastic.

It is becoming clear that all CdTe (Dharmadasa *et al* 2002, 2003), CIGS (Dharmadasa *et al* 2005a), $Al_xGa_{(1-x)}As$ (this work) and thin-film silicon solar cells (Smirnov *et al* 2004, Nobile and Morana 2003) have complex defect structures within the device. The nature of defects will vary from material to material, but their function at any active interface of an electronic device remains the same. They will act as either electron traps or hole traps, and

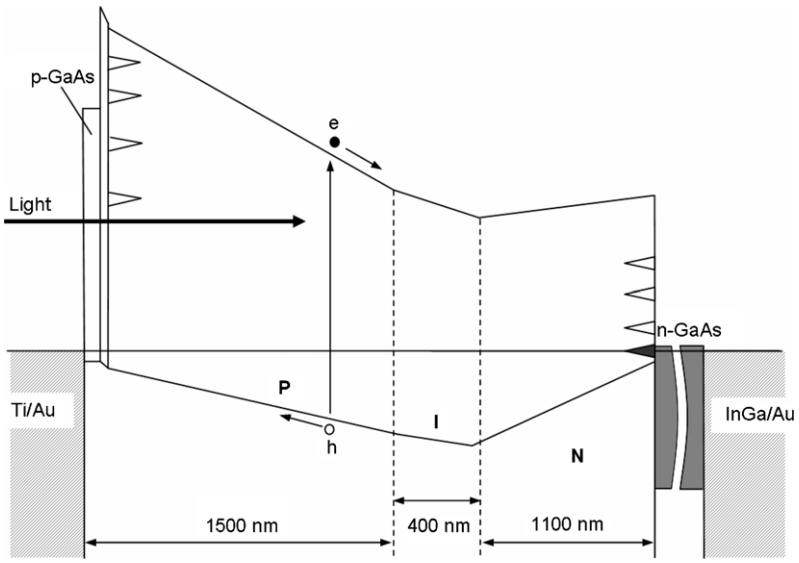


**Figure 10.** Deformation of the energy band diagram, during reverse biasing followed by release of the electrical stress. A second diode is formed at the $Al_xGa_{(1-x)}As$/GaAs interface due to the Fermi level shift to a lower energy level. This band diagram is drawn for a short-circuit configuration.

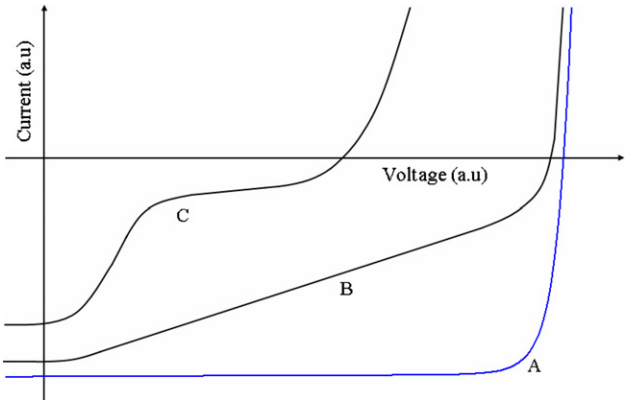


**Figure 11.** Different shapes of *I–V* curves observed for thin-film solar cells based on inorganic materials. Any other shapes between A and C could be observed for different devices.

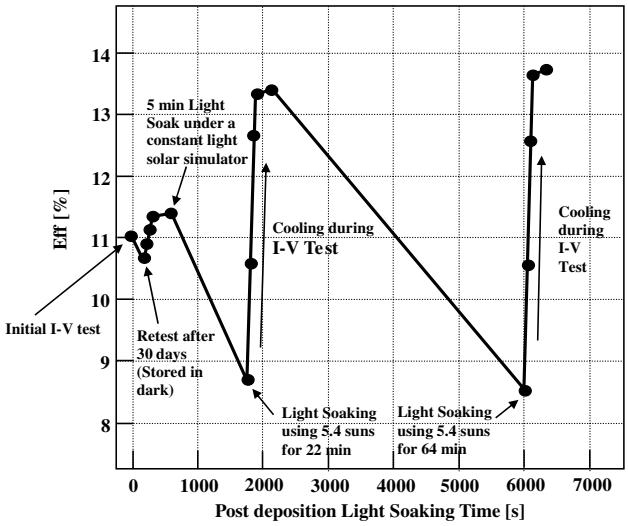


**Figure 12.** The instability of Showa-Shell CIGS solar panels reported by Kushiya (2003, 2004) during stability studies of solar panels.

fill or empty according to the position of the Fermi level at the interface. Therefore, their behaviour and hence the results will be similar irrespective of the semiconductor material used. The defect identifications and their removal or passivation is, therefore, becoming a crucial step in improving reproducibility, performance, stability, yield and lifetime of PV solar cells. This improved understanding of solar cell structures could lead to the achievement of stable, low-cost and highly efficient solar cells in the future. This impact could be seen in all thin-film PV solar cells based on silicon, III–V compounds, CdTe and CIGS, which are currently undergoing intense research and development process.

## Conclusions

The results presented and discussed in this paper lead to the following conclusions. There are drastic effects of defects on thin-film PV solar cell reproducibility, yield, device performance, stability and lifetime. The reproducibility of devices can be severely affected by the presence of several defect levels leading to pinning at different positions and hence producing varying efficiencies (Dharmadasa *et al* 2002). The nature of measured *I–V* characteristics can be affected by external forces such as applied electrical stresses, light soaking and heating or cooling. Because of the effects of a series of defects, the shape of *I–V* curves can be changed due to repeated measurements and the direction of data collection. This is equivalent to the application of external electrical stresses. When a series of defects are present in the active junction area, or in the two electrical contacts, improvement of $V_{oc}$ is observed with a corresponding reduction of $J_{sc}$ values and vice versa. However, the nature of defect structure could also produce weak or strong cell parameters simultaneously for both $V_{oc}$ and $J_{sc}$ parameters. The fill factor and current density values can drastically be affected by the presence of active recombination and generation centres. The above variations are observed for devices with defects of considerable concentration. The undesirable behaviours of solar cells based on inorganic materials are mainly due to defects in the bulk materials, interfaces or the combination of both. In order to produce high-efficiency, stable and long-life solar cells, defect identification, keeping the benign defects and the removal or passivation of detrimental defects are essential. Establishment of these conditions for solar cells based on different materials and structures will lead to considerable improvement of thin-film PV solar cell performance in the future.

## Acknowledgments

Authors acknowledge and thank John Roberts and Geof Hill at the EPSRC central facility in the University of Sheffield for growth and processing of $Al_xGa_{(1-x)}As$-based solar cells. Ayodhya Tiwari and David Brémaud at Zürich Labs, Hari Reehal and Mahanama at the South Bank University, UK, Michael Grätzel, Seigo Ito and Paul Liska at EPFL Labs, Keith Barnham and Daniel Farrell at Imperial College London and Keith Emery and Tim Gessert at NREL are thanked for solar cell measurements for comparison and confirmation purposes. Katsumi Kushiya at Showa Shell is specially thanked for supplying their CIGS materials for full characterization and metal/CIGS interface investigations.

## References

Adachi S 1993 *Properties of Aluminium Gallium Arsenide, EMIS Data Reviews Series No 7* (London: INSPEC)

Contreras M A, Ramanathan K, AbuShama J, Hasoon F, Young D L, Egaas B and Noufi R 2005 *Prog. Photovolt: Res. Appl.* **13** 209

Darmo J, Dubecky F, Hardtdegen H, Hollfelder M and Schmidt R 1998 *J. Cryst. Growth* **186** 13

Dharmadasa I M 2005 *Sol. Energy Mater. Sol. Cells* **85** 293

Dharmadasa I M, Bunning J D, Samantilleke A P and Shen T 2005a *Sol. Energy Mater. Sol. Cells* **86** 373

Dharmadasa I M, Chaure N B, Samantilleke A P and Young J 2003 *GB Patent* 2384621 (filed January 2002 and published July 2003) and *GB Patent* 2397946 (filed January 2002 and published August 2004)

Dharmadasa I M, Chaure N B, Young J and Samantilleke A P 2004 *GB Patent* 02400725 (published 20 October 2004)
Dharmadasa I M, Roberts J S and Hill G 2005b *Sol. Energy Mater. Sol. Cell* **88** 413
Dharmadasa I M, Samantilleke A P, Young J and Chaure N B 2002 *Semicond. Sci. Technol.* **17** 1238
Dharmadasa I M, Tolan G J, Roberts J S, Hill G, Ito S, Liska P and Grätzel M 2006 *Proc. 21st EU Photovoltaic Conf. (Dresden, Germany)* p 257
*EMIS Data Review Series No.2* 1990 *Properties of Gallium Arsenide,* 2nd edn (London: INSPEC)
Green M A, Emery K, King D L, Igari S and Warta W 2005 *Prog. Photovolt: Res. Appl.* **13** 49
Hashizume T and Nagabuchi H 1989 *Semicond. Sci. Technol.* **4** 427
Kushiya K 2003 *Proc. 3rd World Conf. on Photovoltaic Energy Conversion* (*Osaka, Japan, 12–16 May 2003*) p 319
Kushiya K 2004 *Sol. Energy* **77** 717
Nobile G and Morana M 2003 *Sol. Mater. Sol. Cell* **76** 511
Platzer-Björkman C, Kessler J and Stolt L 2003 *Proc. 3rd World Conf. on Photovoltaic Energy Conversion* (*Osaka, Japan, 12–16 May 2003*) p 461
Smirnov V, Reynolds S, Finger F, Main C and Carius R 2004 *Proc. Mat. Res. Soc. Symp.* **808** A9.11.1
Takahashi K, Yamada S and Unno T U.D.C.621.383.51:523.9–7:[546.681′62′19:546. 681′19]